ISSN 1063-7834, Physics of the Solid State, 2015, Vol. 57, No. 2, pp. 412–418. © Pleiades Publishing, Ltd., 2015.
Original Russian Text © R.M. Khusnutdinoff, A.V. Mokshin, I.D. Takhaviev, 2015, published in Fizika Tverdogo Tela, 2015, Vol. 57, No. 2, pp. 393–398.

FULLERENES

Microscopic Dynamics of an Amorphous $C_{60x}/C_{70(1-x)}$ Fullerene Mixture

R. M. Khusnutdinoff*, A. V. Mokshin, and I. D. Takhaviev

Kazan (Volga Region) Federal University, ul. Kremlevskaya 18, Kazan, 420008 Tatarstan, Russia

** e-mail: khrm@mail.ru, anatolii.mokshin@mail.ru*

Received August 25, 2014

Abstract—This paper presents the results of investigation of the propagation mechanism of collective excitations in amorphous $C_{60x}/C_{70(1-x)}$ fullerene mixtures (with equimolar concentration $x = 0.50$), which were obtained using molecular dynamics simulation. The critical glass-transition temperature of the system $T_c = 1548$ K was determined from the change in the behavior of the Wendt–Abraham parameter. Spectral densities of the time correlation functions of the longitudinal $\tilde{C}_L(k, \omega)$ and transverse $\tilde{C}_T(k, \omega)$ currents for a wide region of wave numbers at temperatures below the glass-transition temperature were calculated. It was found that the dynamics of density fluctuations in amorphous $C_{60x}/C_{70(1-x)}$ fullerene mixtures is characterized by two dispersion acoustic-like branches of the longitudinal and transverse polarizations. The influence of polydispersity and form factor of the molecule of the mixture component on the microscopic dynamics of the density fluctuation in multicomponent systems was established.

DOI: 10.1134/S1063783415020183

1. INTRODUCTION

Numerous studies associated with the investigation of the properties of fullerene systems (molecular forms of carbon C_n ($n \in [20; 720]$)) are reduced to the consideration of single-component systems [1–3]. Systems consisting of C_{60} and C_{70} molecules are probably the most studied [4–7]. For example, the authors of [8] experimentally studied electrical conductivity of fullerene crystals C_{60} as a function of the pressure acting on the system. It was found that, as the pressure increases from 100 to 200 kbar, electrical conductivity of the crystal increases by several orders of magnitude. Detailed investigations of the energy spectrum of fullerene C_{60} were recently performed in [9]. An analysis of discrete absorption and emission spectra of fullerene molecules C_{70} in single-crystal toluene was presented in [10]. Numerical and theoretical investigations of the glass transition in C_{60}, C_{70}, and C_{96} single-component fullerene systems were performed using the pair-additive potential of the interatomic interaction in [11]. The authors of [12] performed a comparative analysis of the simulation results for the system of fullerenes C_{60}, where the atomistic model potential of the intramolecular and intermolecular interactions and the Girifalco effective potential of the intermolecular interaction (monatomic model) were used. The investigation was performed for a wide region of pressures (above 200 kbar) in the temperature range from 300 to 1900 K. Good agreement of simulation results with the experimental data for the equilibrium structural characteristics, particularly for the radial distribution function of molecules, equation of state, and series of thermodynamic properties was achieved. This investigation showed the efficiency of the monatomic model of the Girifalco potential when describing the structural characteristics of fullerene systems. Phase diagrams for two different single-component fullerene systems C_{60} and C_{70}, which were calculated based on six model short-range potentials, were presented in [13]. The authors established that binodal curves (liquid–vapor) for these systems are correctly reproduced by calculations performed based on the Girifalco potentials. The effective monatomic Girifalco model was generalized to the case of the C_{60}/C_{70} binary fullerene mixture in [14]. The results of investigations of the microscopic properties of fullerene mixtures C_{60}/C_n ($n = 70, 76, 84, 96$) depending on the concentration of C_{60} molecules were presented in [15].

Despite intense experimental and theoretical investigations of the molecular forms of carbon, the features of the microscopic molecular dynamics in fullerene mixtures in the amorphous phase were almost undisputable in scientific publications.

This paper is devoted to the investigation of the glass transition and microscopic mechanisms of formation of collective excitations in $C_{60x}/C_{70(1-x)}$ fullerene mixtures (at equimolar concentration $x = 0.50$).

2. SIMULATION DETAILS

The system under study consisted of 19652 molecules (by 9826 molecules of fullerenes C_{60} and C_{70} at equimolar concentration $x = 0.50$) arranged in a cubic cell with periodic boundary conditions. The interaction between the molecules was performed using the effective Girifalco potential of the interatomic interaction [14–17]

$$U_{\alpha\beta}(r) = -\frac{\eta_{\alpha\beta}}{s_{\alpha\beta}}\left[\frac{1}{(s_{\alpha\beta}-1)^3} + \frac{1}{(s_{\alpha\beta}+1)^3} - \frac{1}{(s_{\alpha\beta}-\delta_{\alpha\beta})^3} - \frac{1}{(s_{\alpha\beta}+\delta_{\alpha\beta})^3}\right] + \frac{\lambda_{\alpha\beta}}{s_{\alpha\beta}}\left[\frac{1}{(x_{\alpha\beta}-1)^9} + \frac{1}{(s_{\alpha\beta}+1)^9} - \frac{1}{(s_{\alpha\beta}-\delta_{\alpha\beta})^9} - \frac{1}{(s_{\alpha\beta}+\delta_{\alpha\beta})^9}\right]. \quad (1)$$

Here, $s_{\alpha\beta} = r/\sigma_{\alpha\beta}$, $\sigma_{\alpha\beta} = (a_{\alpha+a_\beta})$ is the effective size of the fullerene molecule, $\delta_{\alpha\beta} = (a_\alpha - a_\beta)/(a_\alpha + a_\beta)$, and coefficients $\eta_{\alpha\beta}$ and $\lambda_{\alpha\beta}$ are determined by relationships

$$\eta_{\alpha\beta} = \frac{\varepsilon_{\alpha\beta}\sigma_{\alpha\beta}^6}{12a_\alpha a_\beta(a_\alpha + a_\beta)^4}, \quad \lambda_{\alpha\beta} = \frac{\varepsilon_{\alpha\beta}\sigma_{\alpha\beta}^{12}}{9a_\alpha a_\beta(a_\alpha + a_\beta)^{10}}, \quad (2)$$

where ε is the magnitude, which characterizes the depth of the potential well. Figure 1 shows the intermolecular interaction potential for the $C_{60x}/C_{70(1-x)}$ fullerene mixture.

For convenience, all quantities will be measured in reduced units: lengths—in units of σ, energy—in units of ε, temperature—in units of $k_B T/\varepsilon$, and time—in units of $\tau = \sqrt{m\sigma^2/\varepsilon}$, where m is the mass of the fullerene molecule C_{60} and k_B is the Boltzmann constant.

Molecular dynamics simulations were performed in the NpH ensemble under pressure $p^* = 0.07$ (p = 3.5 MPa) in temperature range $T^* = [0.400–0.625]$ (T = [1287–2011] K). The cooling rate of the system was $\gamma^* = 0.0016$ ($\gamma = 10^{12}$ K/s). Equations of motion for molecules were integrated using the velocity Verlet algorithm with time step $dt^* = 0.001$ (dt = 5.0 fs) [18]. To bring the system into the state of the thermodynamic equilibrium, 50000 time steps were performed. To reduce the computational time, the interaction between the particles at distances $r_{cut} = 2.5\sigma$ was not taken into account.

3. SIMULATION RESULTS

One quantity, which describes the structure of the system under study, is the radial distribution function

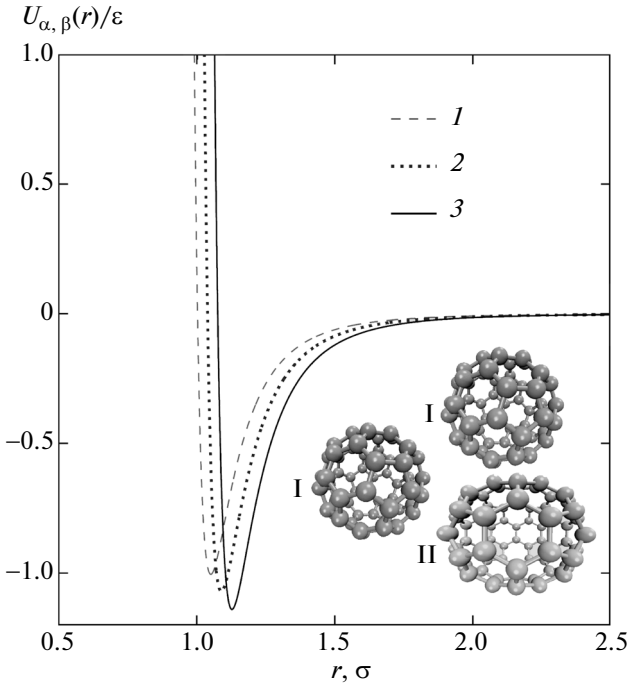

Fig. 1. Interaction potential between fullerene molecules. (*1*) Interaction energy between fullerenes C_{60}, (*2*) interaction energy between molecules C_{70}, and (*3*) interaction energy between molecules C_{60} and C_{70}. Fullerene molecules C_{60} and C_{70} are denoted by symbols I and II, respectively.

of particles $g(r)$ [19, 20]

$$g(r) = x_A b_A^{*2} g_{AA}(r) + x_B b_B^{*2} g_{B,B}(r) + 2\sqrt{x_A x_B} b_A^* b_B^* g_{A,B}(r). \quad (3)$$

Here, $g_{\alpha\beta}(r)$ are partial components of the radial distribution function of molecules [21, 22]

$$g_{\alpha\beta}(r) = \frac{L^3}{N_\alpha N_\beta}\left\langle \sum_{j=1}^{N_a} \frac{n_{j\beta}(r)}{4\pi r^2 \Delta r}\right\rangle, \quad \alpha, \beta \in \{C_{60}, C_{70}\}, \quad (4)$$

which determine the probability density for the arrangement of a pair of molecules in a range from r to $r + \Delta r$. Quantity $n_{j\beta}(r)$ determines the number of molecules of sort β in a spherical layer with thickness Δr at distance r from the jth molecule, L is the edge length of the modeled cell, and N_α and N_β are the numbers of molecules of sorts α and β, respectively. Quantities $x_A = n_A/(n_A + n_B)$ and $x_B = n_B/(n_A + n_B)$ are the concentrations of fullerene molecules C_{60} and C_{70}, respectively; $b_j^* = b_j/(x_A b_A^2 + x_B b_B^2)^{1/2}$ is the normalized scattering length for the molecule of the jth sort (b_A and b_B are scattering lengths of molecules C_{60} and C_{70}, respectively). We consider the scattering length as a quantity commensurable with the size of the C_n

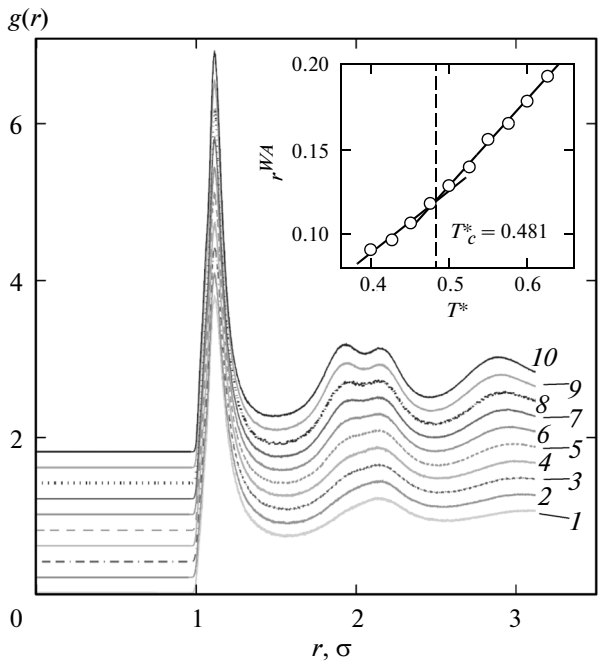

Fig. 2. Temperature dependence of the radial distribution function of fullerene molecules for the $C_{60x}/C_{70(1-x)}$ system ($x = 0.50$). T, ε/k_B: (*1*) 0.625, (*2*) 0.600, (*3*) 0.575, (*4*) 0.550, (*5*) 0.525, (*6*) 0.500, (*7*) 0.475, (*8*) 0.450, (*9*) 0.425, and (*10*) 0.400. The inset shows the temperature dependence of the WendtAbraham parameter.

fullerene molecule: $a_n = a_{60}\sqrt{n/60}$, where a_{60} is the size of the C_{60} fullerene molecule [17].

Figure 2 shows the temperature dependence of the radial distribution function of $C_{60x}/C_{70(1-x)}$ fullerene molecules (at equimolecular concentration $x = 0.50$) under pressure $p^* = 0.07$. It is seen from Fig. 2 that as the temperature lowers, the peaks in the distribution function become more pronounced and the second peak splits. It is known that such features in the behavior of the radial function point to the formation of local structures being characteristic of amorphous materials [23]. To evaluate the transition temperature from the liquid state into the amorphous phase, we calculated the Wendt–Abraham order parameter [24] $r^{WA} = g_{min(1)}/g_{max(1)}$. Here, $g_{max(1)}$ and $g_{min(1)}$ are the values of the first maximum and first minimum of the radial distribution function of the particles, respectively. The temperature dependence of the Wendt–Abraham parameter is presented in inset to Fig. 2. We determined the critical glass-transition temperature of the $C_{60x}/C_{70(1-x)}$ system (at $x = 0.50$), which was $T_c^* = 0.481$ ($T_c^* = 1548$ K), by the intersection of interpolation lines in order parameter r^{WA}.

It should be noted that the authors of [25] found the critical glass-transition temperature for the system of fullerenes C_{60}, which was $T_c^* = 0.342$ ($T_c = 1100$ K) under pressure $p^* = 0.07$ ($p = 3.5$ MPa). Thus, the critical glass-transition temperature of the $C_{60x}/C_{(1-x)}$ fullerene mixture (at $x = 0.50$) turns out considerably higher than T_c for a single-component C_{60} system. It is evident that an increase in the glass-transition temperature can be associated with the presence of nonspherical molecules C_{70} (nonsphericity parameter $S_0 = 0.0033$) in the $C_{60x}/C_{70(1-x)}$ system, which introduces the additional structural disorder. In turn, the latter can also affect the microscopic collective dynamics of the particles.

To analyze the collective properties of the amorphous fullerene mixture, we calculated the spectral density of the time correlation functions of longitudinal (L) and transverse (T) currents

$$\tilde{C}_\alpha(k,\omega) = x_A b_A^* \tilde{C}_\alpha^{AA}(k,\omega) + x_B b_B^{*2} \tilde{C}_\alpha^{BB}(k,\omega) + 2\sqrt{x_A x_B} b_A^* b_B^* \tilde{C}_\alpha^{AB}(k,\omega), \quad \alpha = \{L, T\}, \tag{5}$$

as well as the vibrational density of states of molecules [26]

$$g(\omega) = \frac{\omega}{2\pi(x_A + x_B)} \times \left[\int_{-\infty}^{\infty} [x_A \phi_A(t) + x_B \phi_B(t)] e^{i\omega t} dt\right]^2. \tag{6}$$

Here,

$$\tilde{C}_\alpha^{i,j}(k,\omega) = \frac{1}{t_M}\left|\int_0^{t_M} j_\alpha^{i,j}(k,t) e^{i\omega t} dt\right|^2, \tag{7}$$

where $\alpha = \{L, T\}$ are the partial components of the spectra of the longitudinal and transverse currents and $\phi(t)$ is the velocity autocorrelation function of molecules,

$$\phi_\beta(t) = \frac{\langle \mathbf{v}_\beta(0)\mathbf{v}_\beta(t)\rangle}{\langle \mathbf{v}_\beta(0)\mathbf{v}_\beta(0)\rangle}, \quad \beta \in \{C_{60}, C_{70}\}, \tag{8}$$

angle brackets $\langle ... \rangle$ point to averaging over molecular configurations and $\mathbf{v}_j(t)$ is the velocity vector of the jth molecule in the moment of time t. Current variables, which characterize the propagation of collective excitations in a multiparticle system, are determined by relationships [27, 28]

$$j_L(k,t) = \frac{1}{\sqrt{N}}\sum_{l=1}^{N} (\mathbf{e}_k, \mathbf{v}_l(t)) \exp[-i(\mathbf{k}, \mathbf{r}_l(t))],$$
$$j_T(k,t) = \frac{1}{\sqrt{N}}\sum_{l=1}^{N} |[\mathbf{e}_k, \mathbf{v}_l(t)]| \exp[-i(\mathbf{k}, \mathbf{r}_l(t))]. \tag{9}$$

Here, parentheses and angle brackets denote scalar and vector products, respectively. It should be noted that the spectral density of the time correlation func-

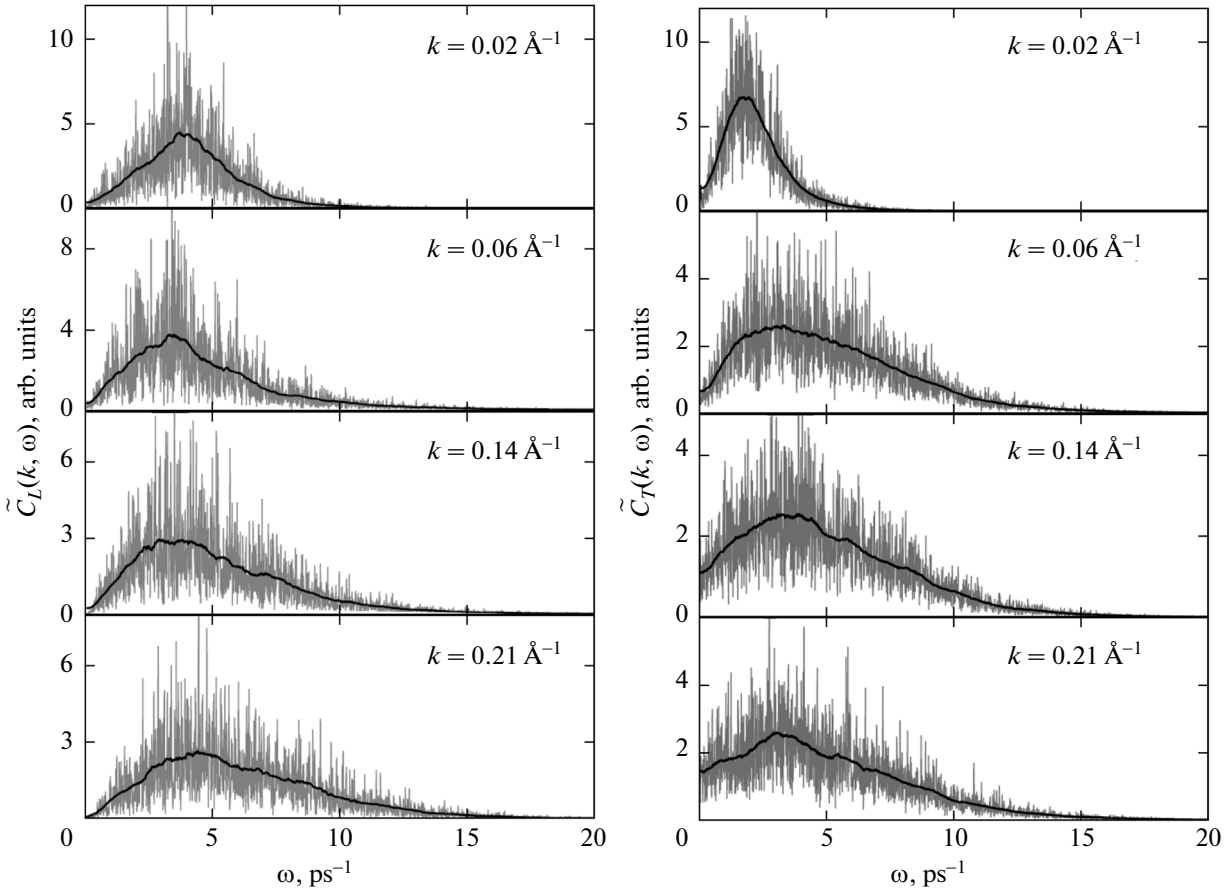

Fig. 3. Spectral densities of the time correlation function for the longitudinal $\tilde{C}_L(k, \omega)$ and transverse $\tilde{C}_T(k, \omega)$ currents for the $C_{60x}/C_{70(1-x)}$ fullerene mixture at temperature $T^* = 0.40$ and pressure $p^* = 0.07$.

tion of the longitudinal current $\tilde{C}_L(k, \omega)$ is associated with the experimentally measured quantity—dynamic structure factor $S(k, \omega)$—by the relationship [29, 30]

$$\tilde{C}_L(k, \omega) = \frac{\omega^2}{\Omega_1^2(k) S(k)} S(k, \omega). \quad (10)$$

Here, $S(k)$ is the static structure factor and $\Omega_1^2(k) = \frac{k_B T}{m} \frac{k^2}{S(k)}$ is the frequency relaxation parameter having dimensionality of the frequency square.

Figure 3 shows spectral densities of the time correlation function of longitudinal $\tilde{C}_L(k, \omega)$ and transverse $\tilde{C}_T(k, \omega)$ currents for the $C_{60x}/C_{70(1-x)}$ fullerene mixture with the equimolar concentration ($x = 0.50$) at temperature $T^* = 0.40$ for a wide range of wave numbers (0.02 Å$^{-1} \le k \le 0.21$ Å^{-1}). These spectral characteristics were calculated based on the obtained results of molecular dynamics simulation. Spectral densities of the time correlation functions of the longitudinal and transverse currents were determined according to expressions (9), (7), and (5).

It is seen from Fig. 3 that propagating collective acoustic excitations are observed in the spectra of the longitudinal current $\tilde{C}_L(k, \omega)$ at $k < 2\pi/\sigma$, where σ is the effective size of the fullerene molecule [31]. At the same time, collective acoustic-like excitations, similar to that manifest themselves in water [32, 33] and other liquids (for example, SiO_2 and GeO_2), the short-range order in which is characterized by tetrahedrality [34, 35], are observed in the spectra of the transverse current $\tilde{C}_T(k, \omega)$.

Figure 4 shows dispersion curves $\omega_c^{(L)}(k)$ and $\omega_c^{(T)}(k)$ for the fullerene mixture, which were obtained based on the analysis of corresponding spectral densities (Fig. 4a) in comparison with the vibrational density of states (Fig. 4b). It is seen from Fig. 4 that the features of the spectra of the longitudinal and transverse currents are also contained in the vibrational density of states (VDOS). In addition, the results presented in Fig. 4 point to the absence of the optical-like

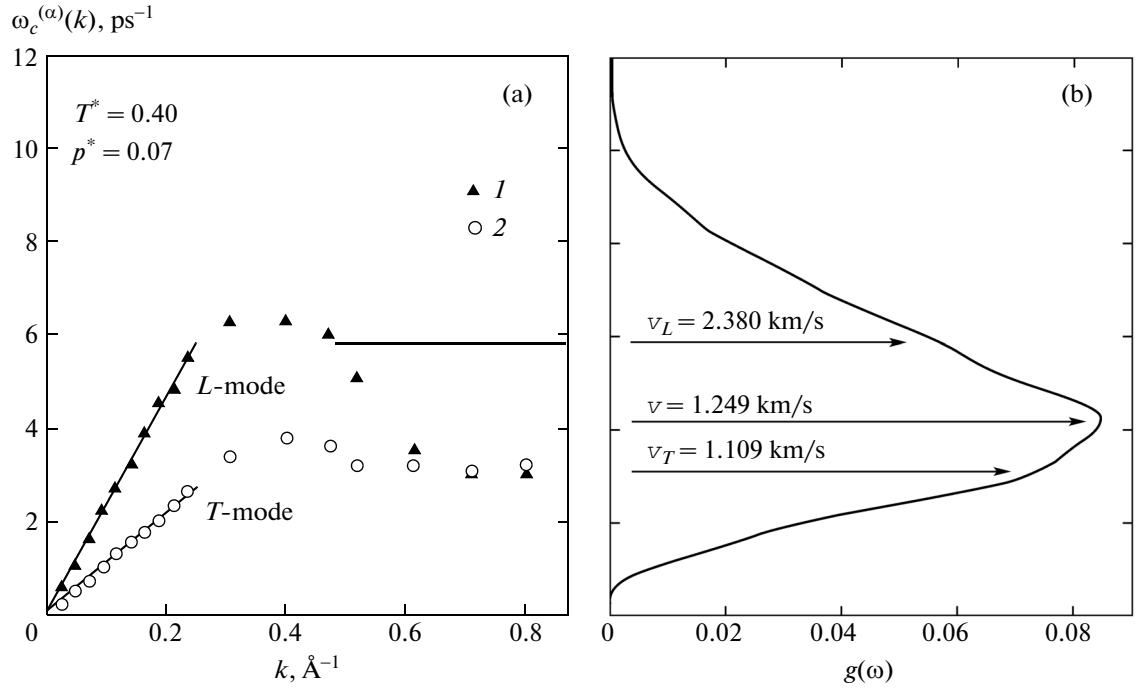

Fig. 4. (a) Dispersion of collective excitations $\omega_c^{(\alpha)}(k)$ of (*1*) longitudinal $\{\alpha \equiv L\}$ and (*2*) transverse $\{\alpha \equiv T\}$ polarizations. The slopes of interpolation straight lines to dispersion dependences in the region of small wave numbers determine velocities of sound with longitudinal v_L and transverse v_T polarizations. (b) Vibrational density of states of fullerene molecules.

branch in the dispersion law for the amorphous fullerene-like mixture.

The interpretation of the results presented in Fig. 4 in comparison with the results [36], where characteristics that describe the VDOS for supercooled water were analyzed, seems to be quite appropriate. Particularly, it was established in [36] that the VDOS for supercooled water has two pronounced peaks. In this case, the VDOS shape can be described/reproduced by the linear combination of three Lorentzian functions. According to [36], they can be associated with vibrational degrees of freedom responsible for deforming the molecules (bending, twisting, and tension). The data of Fig. 4 approach us to a somewhat another interpretation of the features, which manifest themselves in the vibrational density of states. For example, in the region of high wave number k (in the case under consideration, at $k > 0.25$ Å^{-1}), dispersion curves characterize the single-particle collective dynamics. It is seen from Fig. 4 that the molecular motions, which are associated with the formation of acoustic-like waves of the transverse polarization, determine the features of the right (low-frequency) VDOS wing, while molecular vibrational processes, which contribute to the formation of the waves of the longitudinal polarization, form the left (high-frequency) VDOS wing.

Both longitudinal and transverse sound waves can propagate in the crystal [27]. One longitudinal sound wave propagates in the same direction, while two transverse sound waves should be present [28, 29]. Then the average velocity of sound in the solid-state approximation will be determined by the relationship [7, 37]

$$\frac{3}{v^3} = \frac{2}{v_T^3} + \frac{1}{v_L^3}, \tag{11}$$

where

$$v_\alpha = x_A b_A^{*2} v_\alpha^{AA} + x_B b_B^{*2} v_\alpha^{BB} + 2\sqrt{x_A x_B} b_A^* b_B^* v_\alpha^{AB}, \quad \alpha = \{L, T\}, \quad A = C_{60}, \quad B = C_{70}. \tag{12}$$

Values of v_α calculated for the $C_{60x}/C_{70(1-x)}$ fullerene mixture (where $x = 0.25, 0.50, 0.75$) at temperature $T^* = 0.40$ and pressure $p^* = 0.07$, which were calculated according to (11) and (12), are presented in the table.

The tabulated results indicate that an increase in the concentration of molecules C_{60} (in the range $x \in [0.25; 0.75]$) leads to a decrease in the propagation velocity of the acoustic-like wave in this system. For example, the average velocity of sound v decreases more than twofold.

4. CONCLUSIONS

Using molecular dynamics simulation based on the effective model of the intermolecular interaction potential, numerical investigations of the features of

Velocities of sound in the $C_{60x}/C_{70(1-x)}$ fullerene mixture at $T^* = 0.40$ and pressure $p^* = 0.07$

x	Velocity of sound for the longitudinal polarization, km/s				Velocity of sound for the transverse polarization, km/s				Average velocity of sound, km/s
	v_L^{AA}	v_L^{BB}	v_L^{AB}	v_L	v_T^{AA}	v_T^{BB}	v_T^{AB}	v_T	v
0.25	2.430	2.933	2.693	2.692	1.949	1.900	1.900	1.908	2.068
0.50	2.164	2.663	2.335	2.380	1.134	1.133	1.087	1.109	1.249
0.75	2.211	2.139	2.382	2.273	0.868	0.922	0.870	0.882	1.000

the microscopic dynamics of the $C_{60x}/C_{70(1-x)}$ fullerene mixture (at equimolar concentration $x = 0.50$) are performed below the critical glass-transition temperature. Based on the analysis of the spectra of the transverse current, the presence of acoustic-like collective excitations in the amorphous fullerene mixture was established. Propagation velocities of acoustic waves in amorphous $C_{60x}/C_{70(1-x)}$ fullerene mixtures are calculated were calculated at different concentrations of C_{60} molecules ($x = 0.25$, 0.50, 0.75). It was found that an increase in the concentration leads to a noticeable decrease in the propagation velocity of sound in the system.

ACKNOWLEDGMENTS

This study was supported by the subsidy allocated to Kazan Federal University for the state assignment in the sphere of scientific activities. Large-scale molecular dynamics simulations were performed using the computing cluster of the Kazan Federal University and the supercomputer of the Joint Supercomputer Center of the Russian Academy of Sciences.

REFERENCES

1. H. W. Kroto, J. R. Heath, S. C. O'Brien, R. F. Curl, and R. E. Smalley, Nature (London) **318**, 162 (1985).
2. W. Krätschmer, L. D. Lamb, K. Fostiropoulos, and D. R. Huffman, Nature (London) **347**, 354 (1990).
3. V. V. Brazhkin, A. G. Lyapin, S. G. Lyapin, S. V. Popova, R. N. Voloshin, Yu. A. Klyuev, A. M. Naletov, and N. N. Mel'nik, Phys.—Usp. **40** (9), 969 (1997).
4. A. V. Eletskii and B. M. Smirnov, Phys.—Usp. **38** (9), 935 (1995).
5. V. V. Brazhkin and A. G. Lyapin, Phys.—Usp. **39** (8), 837 (1996).
6. V. K. Malinovskii, N. V. Surovtsev, and A. P. Shebanin, JETP Lett. **72** (2), 62 (2000).
7. V. D. Blank, A. A. Nuzhdin, V. M. Prokhorov, and R. Kh. Bagramov, Phys. Solid State **40** (7), 1261 (1998).
8. Yu. A. Osip'yan, V. E. Fortov, K. L. Kagan, V. V. Kveder, V. I. Kulakov, A. N. Kur'yanchik, R. K. Nikolaev, V. I. Postnov, and N. S. Sidorov, JETP Lett. **75** (11), 563 (2002).
9. G. I. Mironov and A. I. Murzashev, Phys. Solid State **53** (11), 2393 (2011).
10. D. K. Nel'son, B. S. Razbirin, V. P. Smirnov, and A. N. Starukhin, JETP Lett. **98** (7), 365 (2013).
11. M. J. Greenall and Th. Voigtmann, J. Chem. Phys. **125**, 194511 (2006).
12. M. C. Abramo, C. Caccamo, D. Costa, G. Pellicane, and R. Ruberto, Phys. Rev. E: Stat., Nonlinear, Soft Matter Phys. **69**, 031112 (2004).
13. P. Orea, J. Chem. Phys. **130**, 104703 (2009).
14. K. Kniaź, J. E. Fischer, L. A. Girifalco, A. R. McGhie, R. M. Strongin, and A. B. Smith III, Solid State Commun. **96**, 739 (1995).
15. R. Ruberto, M. C. Abramo, and C. Caccamo, Phys. Rev. B: Condens. Matter **70**, 155413 (2004).
16. L. A. Girifalco, J. Chem. Phys. **95**, 5370 (1991).
17. V. I. Zubov and I. V. Zubov, J. Phys. Chem. B **109**, 14627 (2005).
18. A. V. Mokshin, A. V. Chvanova, and R. M. Khusnutdinoff, Theor. Math. Phys. **171** (1), 541 (2012).
19. U. Balucani and M. Zoppi, *Dynamics of the Liquid State* (Clarendon, Oxford, 1994).
20. V. F. Turchin, *Slow Neutrons* (Gosatomizdat, Moscow, 1963; Israel Program for Scientific Translations, Jerusalem, 1965).
21. R. M. Khusnutdinoff, A. V. Mokshin, and I. I. Khadeev, J. Surf. Invest. **8** (1), 84 (2014).
22. R. M. Khusnutdinoff and A. V. Mokshin, J. Non-Cryst. Solids **357**, 1677 (2011).
23. A. V. Mokshin, S. O. Zabegaev, and R. M. Khusnutdinoff, Phys. Solid State **53** (3), 570 (2011).
24. R. M. Khusnutdinoff and A. V. Mokshin, Bull. Russ. Acad. Sci.: Phys. **74** (5), 640 (2010).
25. M. C. Abramo, C. Caccamo, D. Costa, and R. Ruberto, J. Phys. Chem. B **108**, 13576 (2004).
26. R. M. Khusnutdinoff and A. V. Mokshin, Physica A (Amsterdam) **391**, 2842 (2012).
27. D. Pines, *Elementary Excitations in Solids* (W. A. Benjamin, New York, 1963).

28. R. M. Khusnutdinoff and A. V. Mokshin, JETP Lett. **100** (1), 39 (2014).

29. A. V. Mokshin, R. M. Yulmetyev, R. M. Khusnutdinov, and P. Hänggi, J. Exp. Theor. Phys. **103** (6), 841 (2006).

30. R. M. Khusnutdinov, A. V. Mokshin, and R. M. Yul'met'ev, J. Exp. Theor. Phys. **108** (3), 417 (2009).

31. A. V. Mokshin, R. M. Yulmetyev, R. M. Khusnutdinoff, and P. Hänggi, J. Phys.: Condens. Matter **19**, 046209 (2007).

32. P. Jedlovszky, G. Garberoglio, and R. Vallauri, Phys. Chem. Chem. Phys. **13**, 19823 (2011).

33. R. M. Khusnutdinoff, Colloid J. **75** (6), 726 (2013).

34. B. Ruzicka, T. Scopigno, S. Caponi, A. Fontana, O. Pilla, P. Giura, G. Monaco, E. Pontecorvo, G. Ruocco, and F. Sette, Phys. Rev. B: Condens. Matter **69**, 100201 (2004).

35. L. E. Bove, E. Fabiani, A. Fontana, F. Paoletti, C. Petrillo, O. Pilla, and I. C. V. Bento, Europhys. Lett. **71**, 563 (2005).

36. P. Jedlovszky, G. Garberoglio, and R. Vallauri, J. Phys.: Condens. Matter **22**, 284105 (2010).

37. J. P. Hansen and I. R. McDonald, *Theory of Simple Liquids* (Academic, New York, 2006).

Translated by N. Korovin